Stress Intensity Factors and Kink Angle of a Crack Interacting with a Circular Inclusion Under Remote Mechanical and Thermal Loadings

Saebom Lee, Seung Tae Choi, Youn Young Earmme*
Department of Mechanical Engineering, Korea Advanced Institute of Science and Technology, Science Town, Daejon 305-701, Korea
Dae Youl Chung
KNGR Project Team, Korea Electric Power Research Institute, Daejon, Korea

A problem of a circular elastic inhomogeneity interacting with a crack under uniform loadings (mechanical tension and heat flux at infinity) is solved. The singular integral equations for edge and temperature dislocation distribution functions are constructed and solved numerically, to obtain the stress intensity factors. The effects of the material property ratio on the stress intensity factor (SIF) are investigated. The computed SIFs are used to predict the kink angle of the crack when the crack grows.

Key Words : Inclusion, Crack, Complex Potential, Stress Intensity Factor, Kink Angle

1. Introduction

Composites deriving advantageous properties from a combination of two or more components are used in numerous structural applications. Ceramics, metals, and polymers are commonly used as a matrix, while inclusions are chosen to tailor the desired properties of composites. For example, it is well known that fibrous composites have a fairly high longitudinal tensile strength and stiffness comparable or superior to those of structural metals (Dvorak, 2000) and brittle materials (Cha et al., 1998). Together with the stresses imposed by external loadings, composite materials must support residual stress due to thermal strain, moisture absorption, inelastic deformation, and phase transformation strain. The residual stress field either alone or in superposition with the external loadings may cause some reliability problems including fiber matrix interface decohesion and matrix cracking.

In order to assess the reliability problems of fiber reinforced composites, the interactions between point singularities (such as edge dislocation or point force), cracks, and inclusions are analyzed via the Muskhelishvili's complex potential method by several researchers. Perlman and Sih (1967) solved the problem of a circular arc interface crack which is located between an inclusion and an infinite matrix under the remote mechanical loading. Atkinson (1972) analyzed an interaction problem between an inclusion and a straight crack, which is embedded in an infinite matrix with radial direction under the remote mechanical loading. Chao and Lee (1996) presented a solution for the same interaction problem with a crack located at arbitrary position under heat flux, which had some critical errors, as found by Chung et al. (2001). On the other hand, Lee et al. (1999) presented a solution for an inclusion with a singularity in an infinite matrix by applying the Suo's complex potential method to circular interface.

* Corresponding Author,
E-mail : y.y.earmme@kaist.ac.kr
TEL : +82-42-869-3013; **FAX** : +82-42-869-3210
Department of Mechanical Engineering, Korea Advanced Institute of Science and Technology, Science Town, Daejon 305-701, Korea. (Manuscript **Received** October 28, 2002; **Revised** April 14, 2003)

In this study, the problem of a matrix crack around an inclusion in an infinite matrix under the remote mechanical loading and heat flux is solved. The effect of an inclusion on a crack is studied by calculating the SIFs at the crack tip as the material property ratios and the crack location vary. The effect of mode mixity, i.e., the ratio of K_I and K_{II}, on the kink angle for the crack growth is also investigated.

2. Problem and Solution

The stresses and displacements are written in terms of the Muskhelishvili's complex potentials $\Phi(z)$ and $\Psi(z)$ (Muskhelishvili, 1953) and the Bogdanoff's temperature potential $\Theta(z)$ (Bogdanoff, 1954) as follows:

$$\sigma_{rr}+\sigma_{\theta\theta}=2[\Phi(z)+\overline{\Phi(z)}] \tag{1}$$

$$\sigma_{rr}+i\sigma_{r\theta}=\Phi(z)+\Omega\left(\frac{1}{\bar{z}}\right)+\bar{z}\left(\bar{z}-\frac{1}{z}\right)\overline{\Psi(z)} \tag{2}$$

$$2\mu\frac{\partial}{\partial\theta}(u_x+iu_y)=iz\left[\kappa\Phi(z)-\Omega\left(\frac{1}{\bar{z}}\right)-\bar{z}\left(\bar{z}-\frac{1}{z}\right)\overline{\Psi(z)}+2\mu B\Theta(z)\right] \tag{3}$$

where, $\Omega(z)=\bar{\Phi}\left(\frac{1}{z}\right)-\frac{1}{z}\bar{\Phi}'\left(\frac{1}{z}\right)-\frac{1}{z^2}\bar{\Psi}\left(\frac{1}{z}\right)$ and $\Theta(z)$ is related to the resultant heat flux Q and the temperature T by $Q=\int_L(q_x dy-q_y dx)=-k\,\mathrm{Im}[\Theta(z)]$ and $T=\mathrm{Re}[\Theta(z)]$. Also, for a plane stress problem, $\kappa=(3-\nu)/(1+\nu)$, $B=A$ while for a plane strain problem, $\kappa=3-4\nu$, $B=(1+\nu)A$ with A being CTE (the Coefficient of Thermal Expansion), ν, Poisson's ratio, and μ, the shear modulus.

As shown in Fig. 1(a), an inclusion with unit radius is perfectly bonded to the matrix containing a crack of length c. Both materials are assumed to be isotropic and linear-thermoelastic. Remote uniform mechanical tension σ^∞ and heat flux q^∞ are applied, which are inclined at the angle of ω and ρ with respect to x-axis, respectively. The solution procedure is divided into two steps. In the first step shown in Fig. 1(b), the problem in which an inclusion is perfectly bonded to the infinite matrix with no cracks under the remote loadings is solved. The loadings are the mechanical tension and the heat flux. Perlman and Sih (1967) presented the solution for this problem under the mechanical tension but it does not satisfy the continuity of displacement and tractions at interface. We reconstructed the solution by the method described in the subsequent section of Problem A. In the second step shown in Fig. 1(c), Problem B, in which an inclusion and a crack are located in an infinite matrix with the prescribed heat flux q_n, tractions σ_n and σ_t on the crack surfaces, is solved. There are not remote loadings. We solved Problem B using the methods by Lee et al. (1999), with q_n, σ_n and σ_t on the crack surface canceling out the

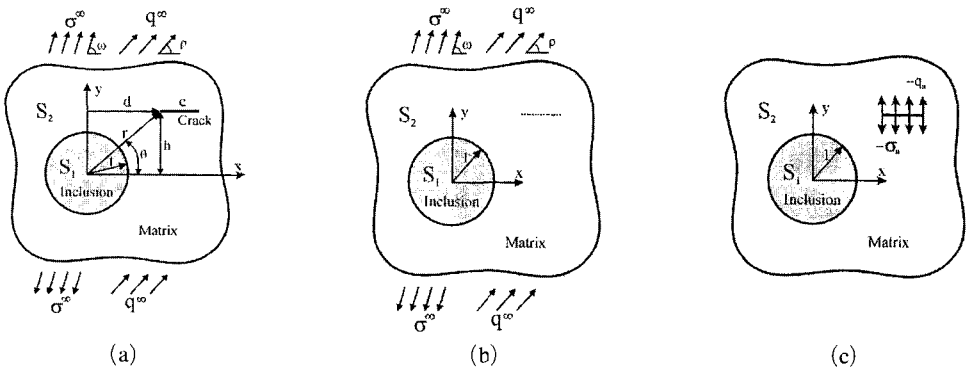

Fig. 1 (a) Interaction between an inclusion and a crack (b) Problem A : an inclusion embedded in an elastic matrix under remote loadings (c) Problem B : an inclusion and a crack. Traction and heat flux are prescribed on the crack faces

respective values from Problem A. A crack is modeled as the sum of the edge and temperature dislocations. In consequence the singular integral equations for dislocation distribution functions are obtained. These equations are transformed into linear algebraic equations for numerical calculation. The stress intensity factors (SIFs) are obtained from the calculated dislocation distribution functions (Hills et al., 1996).

(i) Problem A

In Problem A, we obtain the stress and displacement fields in S_1 and S_2 to get tractions and displacements on the prospective crack surface (shown as dotted line in Fig. 1(b)).

Problem A is independently solved for each loading type. For the remote mechanical tension, Perlman and Sih (1967) presented the solution. Since their work contains some calculation errors, we corrected their solution by the procedure described in Appendix A. For the case of the remote heat flux, the solution can be found in Chung et al. (2001).

Following the procedures described above, the complex potentials for Problem A are found as

$$\Theta^A(z)=\begin{cases}(1-\gamma)\,\Theta_0^A(z), & z\in S_1\\ \Theta_0^A(z)-\gamma\bar{\Theta}_0^A\left(\dfrac{1}{z}\right), & z\in S_2\end{cases} \tag{4}$$

$$\Phi^A(z)=\begin{cases}\dfrac{(1+\alpha)}{(1+\alpha-2\beta)}\dfrac{\sigma^\infty}{4}+\eta_1\Theta_0^A(z), & z\in S_1\\ \dfrac{\sigma^\infty}{4}+\dfrac{(\alpha-\beta)}{1+\beta}\dfrac{\sigma^\infty}{2}\dfrac{e^{2i\omega}}{z^2}+\dfrac{(1+\beta)}{(1+\alpha)}\eta_2\bar{\Theta}_0^A\left(\dfrac{1}{z}\right), & z\in S_2\end{cases} \tag{5}$$

$$\Omega^A(z)=\begin{cases}\dfrac{(1+\alpha)}{(1+\alpha-2\beta)}\dfrac{\sigma^\infty}{4}+\dfrac{1+\beta}{1+\alpha}\dfrac{\sigma^\infty}{2}e^{2i\omega}\dfrac{1}{z^2}, & z\in S_1\\ \dfrac{1+\alpha+2\beta}{1+\alpha-2\beta}\dfrac{\sigma^\infty}{4}+\dfrac{\sigma^\infty}{2}\dfrac{e^{2i\omega}}{z^2}+\eta_1\Theta_0^A(z)-\dfrac{(1+\beta)}{(1+\alpha)}\eta_2\bar{\Theta}_0^A\left(\dfrac{1}{z}\right), & z\in S_2\end{cases} \tag{6}$$

where

$$\Theta_0^A(z)=q^\infty/k_2e^{-i\omega}z$$
$$\alpha=\{\mu_1(\kappa_2+1)-\mu_2(\kappa_1+1)\}/\{\mu_1(\kappa_2+1)+\mu_2(\kappa_1+1)\}$$
$$\beta=\{\mu_1(\kappa_2-1)-\mu_2(\kappa_1-1)\}/\{\mu_1(\kappa_2+1)+\mu_2(\kappa_1+1)\}$$
$$\eta_1=\{B_2-(1-\gamma)B_1\}\{2\mu_1\mu_2/(\mu_1+\mu_2\kappa_1)\}$$
$$\eta_2=\{B_2\gamma\}\{2\mu_1\mu_2/(\mu_2+\mu_1\kappa_2)\}$$
$$\gamma=(k_1-k_2)/(k_1+k_2).$$

(ii) Problem B

A crack is modeled as the sum of the edge and temperature dislocations. Problem B is independently solved for each dislocation type. Integrating the solution for a single edge dislocation (Lee et al., 1999), we can obtain the solution for the edge dislocations. Chao and Lee (1996) obtained the solution for the temperature dislocation with some errors, in which the stress and displacement fields are infinite at $z=0$. The corrected solution can be found in Chung et al. (2001). As a result, the complex potentials for Problem B are found as

$$\Theta^B(z)=\begin{cases}(1-\gamma)\,\Theta_0^B(z), & z\in S_1\\ \Theta_0^B(z)-\gamma\bar{\Theta}_0^B\left(\dfrac{1}{z}\right), & z\in S_2\end{cases} \tag{7}$$

$$\Phi^B(z)=\begin{cases}(1+\Lambda)\,\Phi_0(z)+\eta_1\Theta_0^B(z)+(1+\Lambda)f(z)+\dfrac{g(z)}{1-\beta}, & z\in S_1\\ \Phi_0(z)+\Pi\Omega_0^B(z)+\eta_2\bar{\Theta}_0^B\left(\dfrac{1}{z}\right)+f(z)+\dfrac{g(z)}{1+\beta}, & z\in S_2\end{cases} \tag{8}$$

$$\Phi^B(z)=\begin{cases}(1+\Pi)\,\Omega_0(z)+\eta_2\bar{\Theta}_0^B\left(\dfrac{1}{z}\right)+\dfrac{g(z)}{1+\beta}, & z\in S_1\\ \Omega_0(z)+\Lambda\Phi_0(z)+\eta_1\Theta_0^B(z)+\Lambda f(z)+\dfrac{g(z)}{1-\beta}, & z\in S_2\end{cases} \tag{9}$$

where

$$\Theta_{B0}(z)=\frac{1}{2\pi i}\int_L b_0(s)\ln(z-s)\,ds$$
$$\Phi_0(z)=\frac{\mu_2}{\pi i(\kappa_2+1)}\int_L\frac{b_x(s)+ib_y(s)}{(z-s)}\,ds$$
$$\Omega_0(z)=\frac{\mu_2}{\pi i(\kappa_2+1)}\left\{\int_L\frac{(z^2+1)\,b_x(s)-(z^2-1)\,ib_y(s)}{z(z\bar{s}-1)}\,ds-\int_L\frac{(z-s)\,[b_x(s)-ib_y(s)]}{(z\bar{s}-1)^2}\,ds\right\}$$
$$\Lambda=(\alpha+\beta)/(1-\beta)$$
$$\Pi=(\alpha-\beta)/(1+\beta)$$
$$f(z)=-\frac{2\beta}{1+\alpha-2\beta}\mathrm{Re}[\Phi_0(0)]+i\frac{2\alpha}{1-\alpha}\mathrm{Im}[\Phi_0(0)]-\frac{1-\beta}{1+\alpha}(\eta_1-\eta_2)\,\Theta_{B0}(0)+\frac{1+\beta}{1+\alpha}\eta_2\frac{\bar{\Theta}'_{B0}(0)}{z}$$
$$g(z)=\frac{(1+\alpha)(3\beta-\alpha)}{1+\alpha-2\beta}\mathrm{Re}[\Phi_0(0)]-i\frac{(\alpha+\beta)(1+\alpha)}{1-\alpha}\mathrm{Im}[\Phi_0(0)]-(1+\beta)\eta_2\frac{\bar{\Theta}'_{B0}(0)}{z}.$$

In the above, $b_0(s)$ is the distribution function of the thermal dislocations, and $b_x(s)$, $b_y(s)$ are x and y components of the distribution function of the edge dislocations, respectively. They are determined from the following conditions:

$$\sigma_n^A+\sigma_n^B+i(\sigma_t^A+\sigma_t^B)=0, \quad \text{along the crack line } L \tag{10}$$

$$q_n^A+q_n^B=0, \quad \text{along the crack line } L \tag{11}$$

$$\int_L b_0(s)\,ds=0 \tag{12}$$

$$\int_L [b_x(s)+ib_y(s)]\,ds-B_2\int_L\left[\int b_0(\xi)\,d\xi\right]ds=0 \tag{13}$$

Equation (10) represents the condition of traction free on crack surface, Eq. (11) the insulated crack, and Eq. (12) and Eq. (13) the single-valuedness of temperature and displacement dislocations, respectively. The subscript 2 in B_2 means the value B corresponding to material 2 (the matrix), while the subscripts (n and t) denote the normal and tangential components, respectively. The singular integral equations are obtained from Eqs. (10)~(13). For numerical calculation, we transform these singular integral equations into a set of linear algebraic equations by Gauss-Chebyshev quadrature formulae. Once if $b_0(s)$, $b_x(s)$, and $b_y(s)$ are calculated, the SIFs are easily obtained (Hills et al, 1996).

3. Numerical Results and Discussion

Maple 7 (Monagan et al., 2001) is used for programming the calculation code. We construct a set of linear algebraic equations for each dislocation distribution functions, $b_0(s)$ $b_x(s)$, and $b_y(s)$ by dividing every integration interval into five intervals. The SIFs at the various locations of a crack are final output of the numerical calculations. And the SIFs are normalized by

$$K_{I0}=\sigma^\infty\sqrt{\pi c/2} \tag{14}$$

under the remote mechanical tension which is K_I of the homogeneous material with $\omega=\pi/2$ and

$$K_{II0}=\frac{B\mu c^{3/2}\sqrt{\pi}}{\sqrt{2}\,(1+\kappa)}\,\frac{q^\infty}{k} \tag{15}$$

under the remote heat flux which is K_{II} of the homogeneous material with $\rho=\pi/2$ (Florence and Goodier, 1960). The geometry used for the calculation is shown in Fig. 1(a). The SIFs are calculated at the left tip of the crack. The location of the left crack tip is $(d,\ h)$ in Cartesian or $(r,\ \theta)$ in polar coordinates. Other variables are found in the Section 2.

3.1 Verification

In order to verify our solution, we performed the computations of the following cases.

(i) If all material properties of S_1 and S_2 are identical, then the material would be homogeneous. And if the crack is well far from the inclusion, it would behave as if that in the homogeneous material. We compare the calculated values in the two above cases with the theoretical values (Eqs. (14)~(15)) for the homogeneous S_2 material. In result, the calculated SIFs are identicaly confirmed to the theoretical values.

(ii) The calculated SIFs are compared to FEM values. The inclusion of unit radius is located at

Table 1 Mechanical properties used in FEM

properties \ materials		Inclusion	matrix
		boron	epoxy
shear modulus	μ	172.5 GPa	1.24 GPa
Poissons ratio	ν	0.2	0.4
CTE	A	5.0 μm/mK	57.6 μm/mK
heat conductivity	k	18.2 W/mK	0.45 W/mK

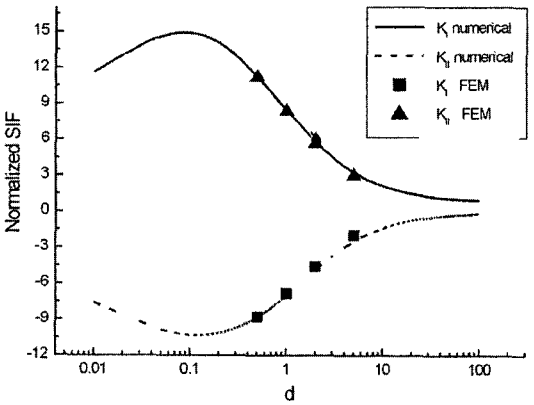

Fig. 2 Normalized SIFs under the remote heat flux

the origin with the crack of length $c=0.2$ along the x-axis ($h=0$). The position of the left crack tip is (d, 0). Remote uniform heat flux q^{∞} is applied with $\rho=\pi/4$. The materials are considered as the Boron and the epoxy. Their properties are listed in Table 1. and the results are shown in Fig. 2. The solid and dotted lines are the numerically calculated results for K_I and K_{II}, respectively. The symbols, ■ and ▲ are respectively FEM values. It is noted that the both results are indistinguishable.

3.2 Calculations

We first investigate the effect of various parameters on the SIFs, and then analyze the crack behaviors in engineering composite materials. The parameters which affect the SIFs are the material property ratios γ_G, γ_A, γ_k to be defined later, the magnitudes σ^{∞}, q^{∞} and inclined angles ω, ρ of the remote loadings, the length of the crack c, and the relative position of the crack tip to the inclusion (d, h) or (r, θ). Since we are concerned about the micro-cracks around an inclusion, the length of the crack is chosen to be the same with the size of the inclusion. It is found that the effect of the larger than unit crack length c is negligible for the our cases. The effect of the material property ratios and the remote loading angles are investigated in the Section 3.2.1 by obtaining the SIFs for various ratios of the material properties of the inclusion and matrix under the selected remote loading angles. The calculated SIFs are plotted as a function of the location of the crack. Since the effect of considered here due to the normalization of the remote loadings would be in proportion to the magnitude, it is not the calculated SIFs by K_{I0} and K_{II0} (Eqs. (14)~(15)). For application examples, we obtain the SIFs and the kinking angle for a crack in the engineering composite materials in the Section 3.2.2 where the ceramic particulate-reinforced metal matrix composite, SiC-Al (Han et al., 1999) and the metal particle-reinforced ceramic matrix composite, Ni-Al_2O_3 (Jin and Batra, 1999) are selected.

Each of all figures (Figs. 3~20) is classified into three classes (a), (b), and (c) which are labeled at the bottom of each figure (such as Fig. 3(a), Fig. 5(b), etc.) according to the location of the crack. In the class (a), the crack is on x-axis (that is, $h=0$ and d arbitrary), in the class (b) the crack tip is located on y-axis ($d=0$ and h arbitrary), and in the class (c) θ varies with the same distance, $r=\sqrt{(d^2+h^2)}=1.1$. It should be noted that the negative values of K_I in all the figures are meaningless, since the crack surface contacts and, they are regarded as zero. However, we retain negative values since in combination of the remote mechanical tension and heat flux, the total resultant K_I can be positive.

3.2.1 Effect of material property ratios and remote loading angles

The material properties affecting the solution are the shear modulus μ, the CTE A, the thermal conductivity k, and Poisson's ratio v. The effect of is not presented here since its effect on the SIFs is found to be negligible. Hereafter, we use the γ with no subscript as a generic term of the ratio of material properties. The ratio of each material property is defined as follows:

$$\gamma_G=\mu_1/\mu_2 \tag{16}$$

$$\gamma_A=A_1/A_2 \tag{17}$$

$$\gamma_k=k_1/k_2 \tag{18}$$

In Eqs. (16)~(18), γ_G, γ_A, and γ_k are the shear modulus ratio, the CTE ratio, and the thermal conductivity ratio, respectively. Subscript 1 and 2 indicate respective materials (the inclusion and matrix as in Fig. 1). The remote loading angles ω and ρ are selected to be $\pi/2$ and $\pi/4$. The calculated SIFs are shown in Figs. 3~10. Under each remote loading condition, the SIFs for two values of γ (=10, 0.1) are plotted in the same figure. The SIFs for the case of $\gamma=10$ are denoted by the solid points and while the case of $\gamma=0.1$ by the open points (only the results for $\gamma=10$ and 0.1 are presented here since for other values of $\gamma(>1)$ we obtained the similar results to $\gamma=10$ and for $\gamma(<1)$ to $\gamma=0.1$). The effects of γ_G under the mechanical tension are shown in Figs. 3~4, in which $\gamma_A=\gamma_k=1$. The effects of γ_G, γ_A, and γ_k under the heat flux are shown in Figs.

5~6, Figs. 7~8, and Figs. 9~10, respectively. It is noted here that when the effect of a single material property ratio is investigated, all other material property ratios are set to be unit.

As shown in Figs. 3~10 with labels (a) and (b), e.g., Fig. 3(a), 3(b), Fig. 10(b), etc., the

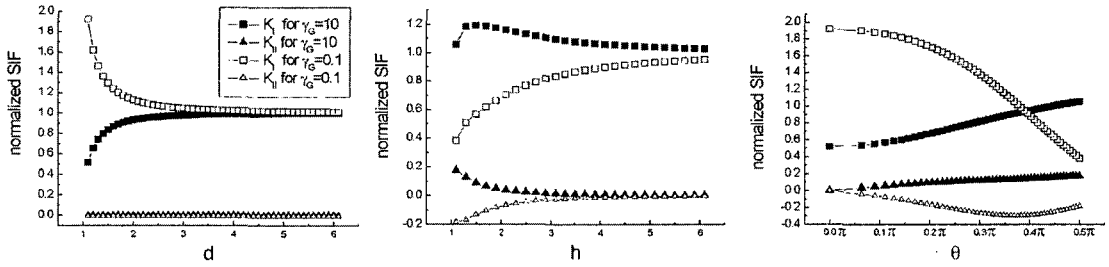

Fig. 3 Effect of γ_G on the SIFs under $\sigma^\infty=1$, $\omega=\pi/2$, $q^\infty=0$, where (a) $h=0$ (b) $d=0$ (c) $r=1.1$

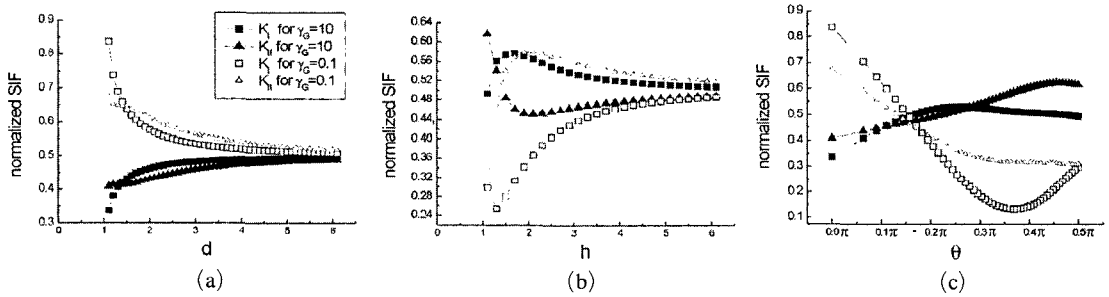

Fig. 4 Effect of γ_G on the SIFs under $\sigma^\infty=1$, $\omega=\pi/4$, $q^\infty=0$, where (a) $h=0$ (b) $d=0$ (c) $r=1.1$

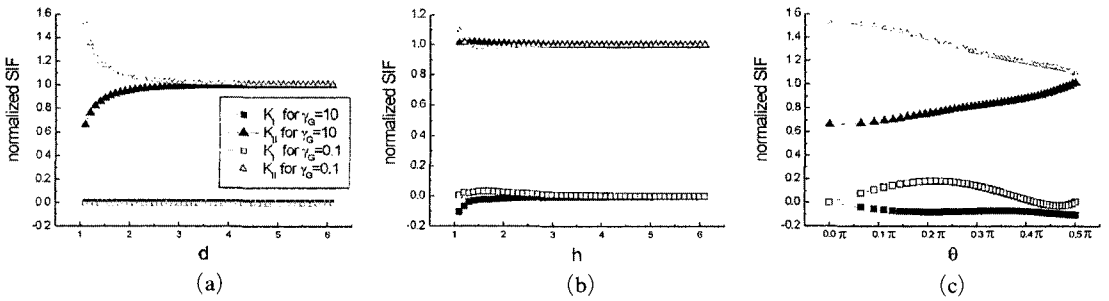

Fig. 5 Effect of γ_G on the SIFs under $\sigma^\infty=0$, $q^\infty=1$, $\rho=\pi/2$, where (a) $h=0$ (b) $d=0$ (c) $r=1.1$

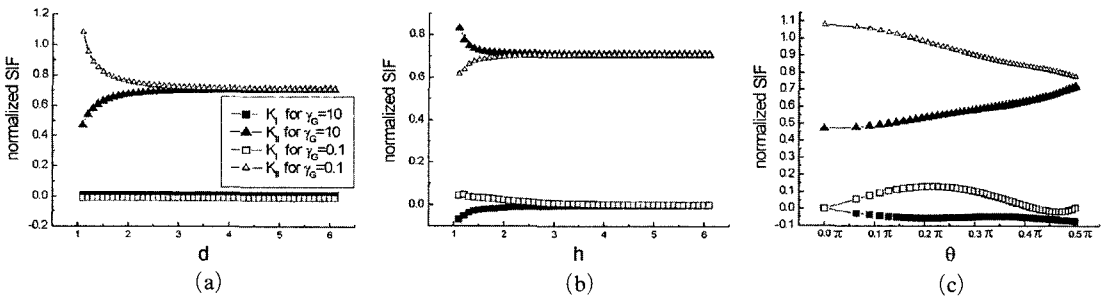

Fig. 6 Effect of γ_G on the SIFs under $\sigma^\infty=0$, $q^\infty=1$, $\rho=\pi/4$, where (a) $h=0$ (b) $d=0$ (c) $r=1.1$

normalized SIF seems to converge to a single value as the distance of the crack, γ from the inclusion becomes larger. For all kinds of the material properties, the tendencies in the variations of SIFs for $\gamma=10$ and $\gamma=0.1$ are opposite to each other.

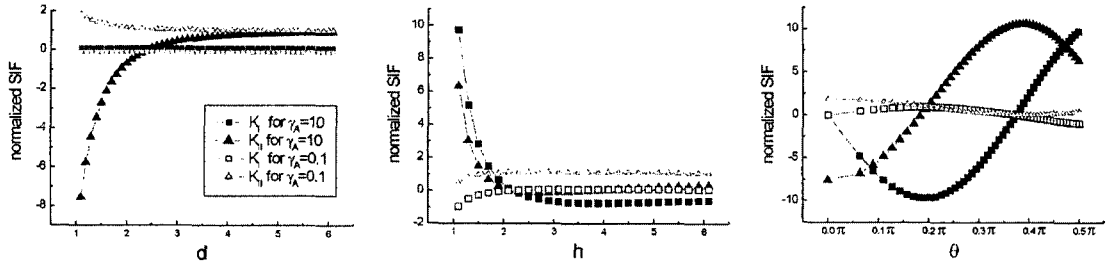

Fig. 7 Effect of γ_A on the SIFs under $\sigma^{\infty}=0$, $q^{\infty}=1$, $\rho=\pi/2$, where (a) $h=0$ (b) $d=0$ (c) $r=1.1$

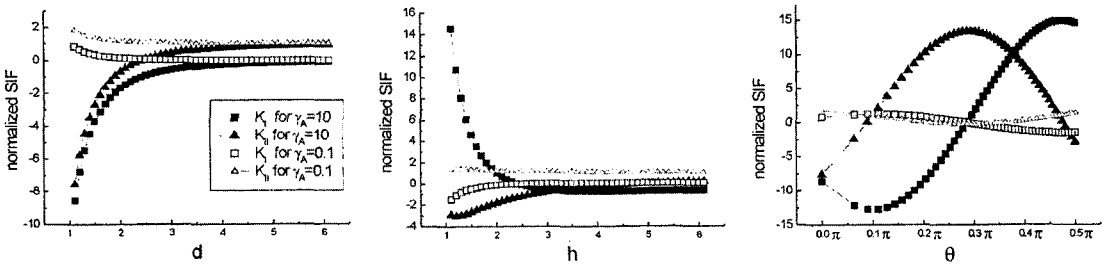

Fig. 8 Effect of γ_A on the SIFs under $\sigma^{\infty}=0$, $q^{\infty}=1$, $\rho=\pi/4$, where (a) $h=0$ (b) $d=0$ (c) $r=1.1$

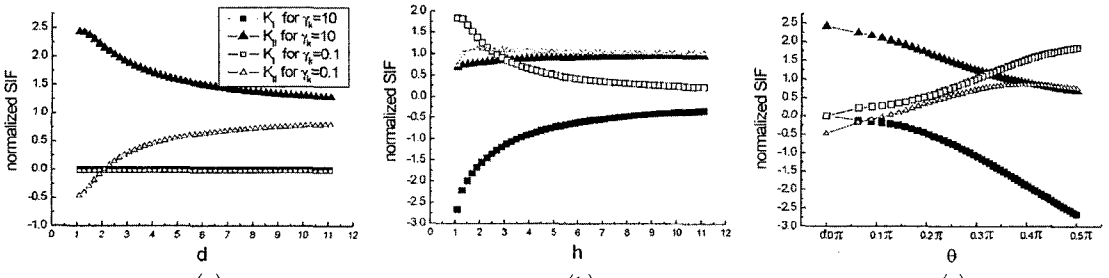

Fig. 9 Effect of γ_k on the SIFs under $\sigma^{\infty}=0$, $q^{\infty}=1$, $\rho=\pi/2$, where (a) $h=0$ (b) $d=0$ (c) $r=1.1$

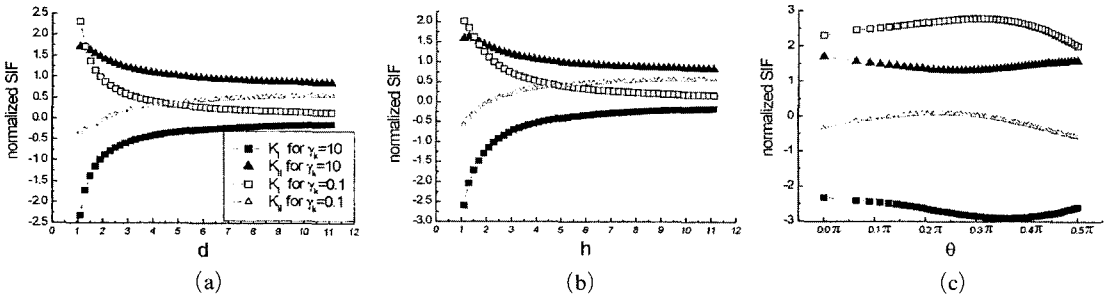

Fig. 10 Effect of γ_k on the SIFs under $\sigma^{\infty}=0$, $q^{\infty}=1$, $\rho=\pi/4$, where (a) $h=0$ (b) $d=0$ (c) $r=1.1$

To discuss more closely the effect of the parameters, we classified the cases into (i) and (ii) as follows :

(i) Under the remote mechanical tension ($\sigma^{\infty}=1$, $q^{\infty}=0$)

The SIFs for $\omega=\pi/2$ are shown in Fig. 3 and for $\omega=\pi/4$ in Fig. 4. K_I for the case of $\gamma_G=10$ appreciably decreases as the crack tip on x-axis approaches the inclusion as shown in Fig. 3(a) and Fig. 4(a), while it slightly decreases, as shown in Fig. 3(b) and Fig. 4(b), as the crack tip on y-axis approaches to the inclusion. In case of $\omega=\pi/2$, K_{II} at the crack tip on x-axis is definitely zero as in Fig. 3(a). But it is not zero at the crack tip on y-axis (Fig. 3(b)). We can appreciate the effect of the remote loading angles from the difference in Fig. 3 and Fig. 4. Although the tendenciy is similar, the magnitude of K_I dominates for $\omega=\pi/2$ while K_I and K_{II} show almost same magnitudes for $\omega=\pi/4$.

(ii) Under the remote heat flux ($\sigma^{\infty}=0$, $q^{\infty}=1$)

The results are shown in Figs. 5~10. The difference in the temperature between the upper and the lower surfaces of an insulated crack occurs under the remote heat flux. K_{II} is, therefore, dominant, as in the homogeneous case (Chao and Lee, 1996). To discuss more closely the effect of γ_G, γ_A, and γ_k, we present as follows :

- Effect of γ_G ($\rho=\pi/2$ in Fig. 5 and $\rho=\pi/4$ in Fig. 6)

  Compared to the cases of γ_A or γ_k (Figs. 7~10), the variations of SIFs are not relatively severe. The effect of the loading angle ρ is negligible with comparing Fig. 5 and Fig. 6.
- Effect of γ_A ($\rho=\pi/2$ in Fig. 7 and $\rho=\pi/4$ in Fig. 8)

  It is seen in Fig. 7(a) and Fig. 7(b) that the magnitude of K_{II} is very large when the crack is located in the vicinity of the inclusion, and small as the crack becomes more distant from the inclusion. This means that the effect of γ_A on the SIFs is significant near the inclusion.
- Effect of γ_k ($\rho=\pi/2$ in Fig. 9 and $\rho=\pi/4$ in Fig. 10)

  K_{II} for the case of $\gamma_k=10$ increases as the crack tip on x-axis approaches to the inclusion as shown in Fig. 9(a) and Fig. 10(a). As seen in Fig. 9, the convergences of SIFs for γ_k are poor in comparison with the cases of γ_G and γ_A. It may be due to the fact that the effect of γ_k on the SIFs is long-ranged compared to γ_G and γ_A.

3.2.2 Composites

In this subsection, we consider two typical material combinations of, SiC(inclusion)-Al (matrix) and Ni(inclusion)-Al_2O_3(matrix) composites and compute the SIFs as shown in Figs. 11~14. The kinking angle Ω which is obtained from the calculated SIFs in the composites is shown in Fig. 17~20. The putative crack segment kinking out the plane of the crack at an angle Ω shown in Fig. 15 is referred to as the kink crack. The original crack will be referred to as the parent crack. The kinking angle Ω for which $K_{II}^{t}=0$ is plotted as a function of Ψ in Fig. 16 which was taken from Hutchinson and Suo (1990). Here K_{II}^{t} is the mode II SIF at the tip of the kink crack, and Ψ is the measure of the mode II to the mode I SIF for the parent crack defined by $\Psi=\tan^{-1}(K_{II}/K_I)$. The material properties of SiC, Al, Ni, and Al_2O_3 are listed in Tables 2 and 3. The material property ratios are $\gamma_G=7$, $\gamma_A=0.19$, $\gamma_k=0.70$, for SiC-Al and $\gamma_G=0.47$, $\gamma_A=2.47$, $\gamma_k=1.52$ for Ni-Al_2O_3. Calculations are

Table 2 Mechanical properties of SiC and Al

properties \ materials		Inclusion	matrix
		SiC	aluminum
shear modulus	μ	184.2 GPa	26.3 GPa
Poissons ratio	ν	0.14	0.33
CTE	α	4.5 μm/mK	23.6 μm/mK
heat conductivity	k	125.6 W/mK	180 W/mK

Table 3 Mechanical properties of Ni and Al_2O_3

properties \ materials		Inclusion	matrix
		Ni	Al_2O_3
shear modulus	μ	76 GPa	161.4 GPa
Poissons ratio	ν	0.31	0.27
CTE	A	13.1 μm/mK	5.3 μm/mK
heat conductivity	k	60.7 W/mK	40 W/mK

performed for the respective remote loadings with $\omega=\rho=\pi/2$ and the results are summarized as follows:

(i) Stress intensity factors

Under the remote mechanical tension, the SIFs for the crack in SiC-Al and Ni-Al_2O_3 (Fig. 11

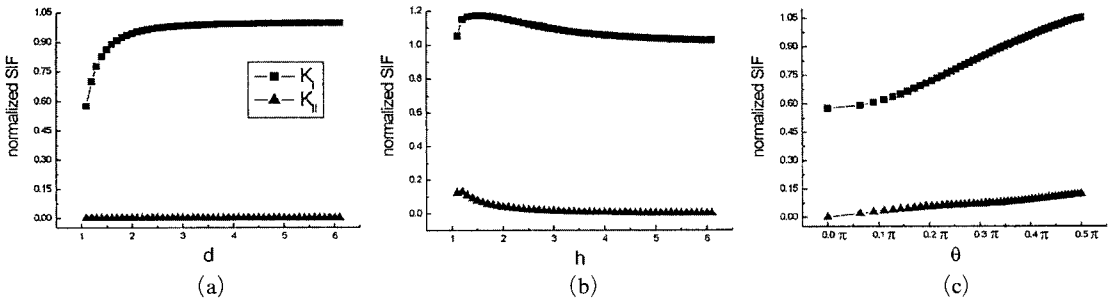

Fig. 11 The SIFs for the crack in SiC-Al under $\sigma^{\infty}=1$, $\omega=\pi/2$, $q^{\infty}=0$, where (a) $h=0$ (b) $d=0$ (c) $r=1.1$

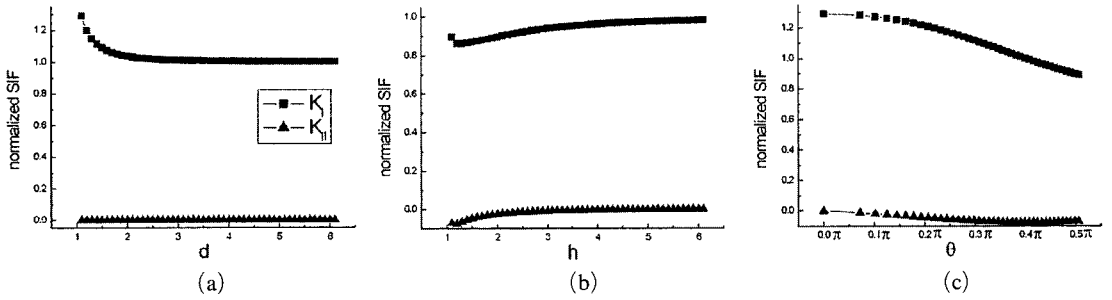

Fig. 12 The SIFs for the crack in Ni-Al_2O_3 under $\sigma^{\infty}=1$, $\omega=\pi/2$, $q^{\infty}=0$, where (a) $h=0$ (b) $d=0$ (c) $r=1.1$

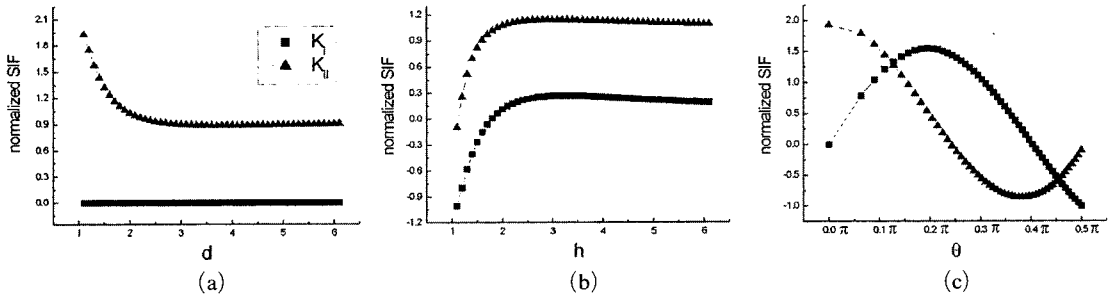

Fig. 13 The SIFs for the crack in SiC-Al under $\sigma^{\infty}=0$, $q^{\infty}=1$, $\rho=\pi/2$ where (a) $h=0$ (b) $d=0$ (c) $r=1.1$

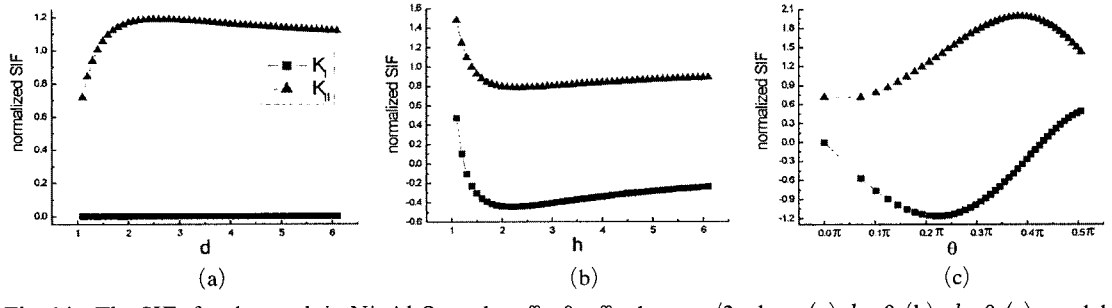

Fig. 14 The SIFs for the crack in Ni-Al_2O_3 under $\sigma^{\infty}=0$, $q^{\infty}=1$, $\rho=\pi/2$ where (a) $h=0$ (b) $d=0$ (c) $r=1.1$

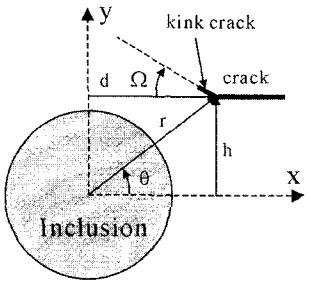

Fig. 15 Conventions and geometry

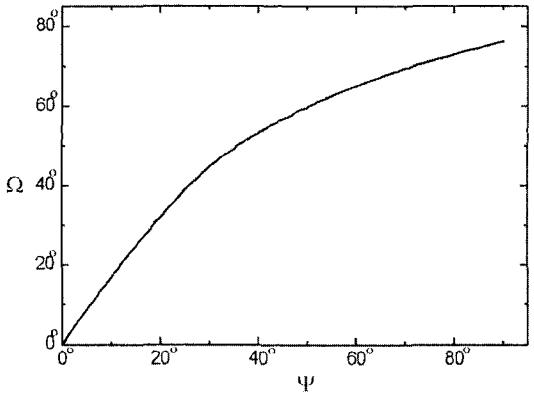

Fig. 16 Kink angle, Ω as predicted by $K_{II}^{t}=0$, where $\Psi=\tan^{-1}\left(\frac{K_{II}}{K_I}\right)$

and Fig. 12, respectively) are very similar to those for the case of $\gamma_G=10$ and $\gamma_G=0.1$ in Fig. 3, respectively. For SiC-Al under the remote heat flux, (shown in Fig. 13), it is found that both K_I and K_{II} are zero at the value of $h\simeq 1.2$ (Fig. 13 (b)) in which we set $K_I=0$ if the value of K_I is negative.

(ii) Kink angles

As seen in Fig. 16, if the value of K_{II} is zero, Ω is zero irrespectively of the value of K_I (the crack will not kink). If K_I vanishes with non-vanishing K_{II}, the crack kinks with the maximum magnitude of $\Omega(\approx 73.5°)$. Under the remote mechanical tension, Ω for the parent crack on x-axis in SiC-Al is zero as shown in Fig. 17(a). Ω is positive for other locations of the crack. It means that the crack in SiC-Al kinks away from the inclusion when a kinking occurs. As shown in Fig. 18(b) (the crack tip on y-axis) and Fig. 18 (c) (the crack tip at a fixed distance of $r=1.1$), the kink crack in Ni-Al_2O_3 grows toward the inclusion, while the crack on x-axis (Fig. 18(a)) does not kink. Under the remote heat flux, the value of Ω is maximum at most locations of the

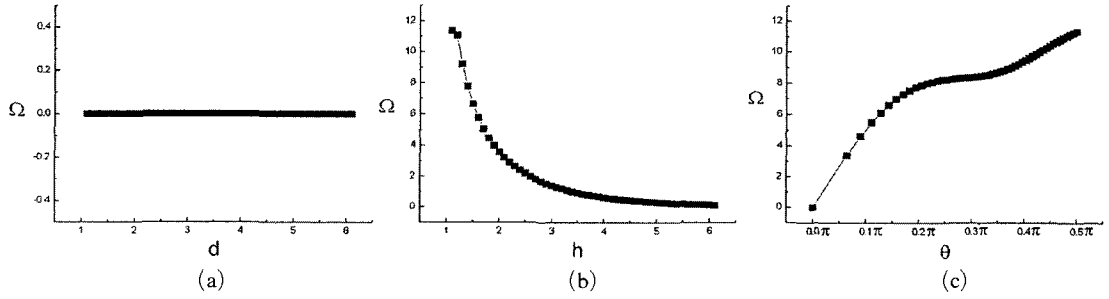

Fig. 17 Kink angle for the crack in SiC-Al under $\sigma^{\infty}=1$, $\omega=\pi/2$, $q^{\infty}=0$, where (a) $h=0$ (b) $d=0$ (c) $r=1.1$

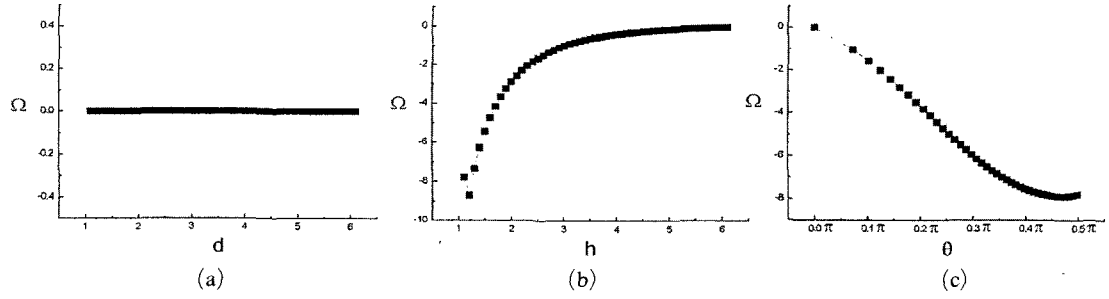

Fig. 18 Kink angle for the crack in Ni-Al_2O_3 under $\sigma^{\infty}=1$, $\omega=\pi/2$, $q^{\infty}=0$, where (a) $h=0$ (b) $d=0$ (c) $r=1.1$

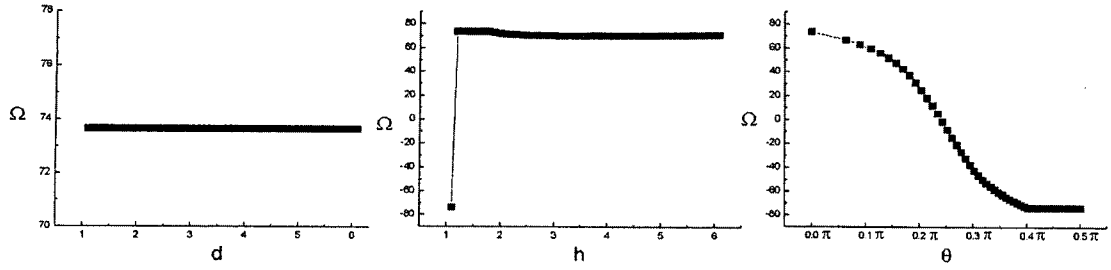

Fig. 19 Kink angle for the crack in SiC-Al under $\sigma^{\infty}=0$, $q^{\infty}=1$, $\rho=\pi/2$, where (a) $h=0$ (b) $d=0$ (c) $r=1.1$

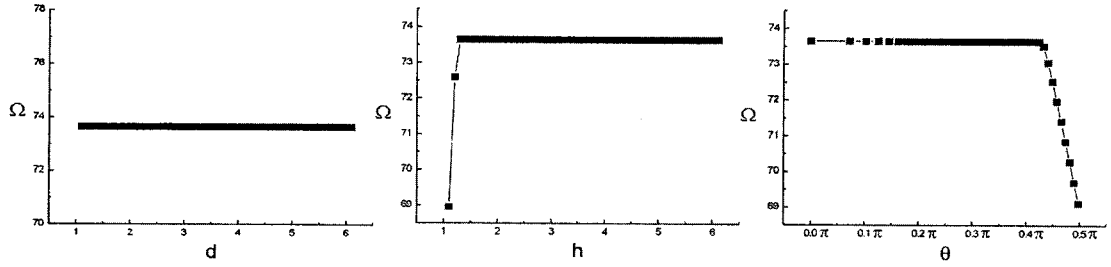

Fig. 20 Kink angle for the crack in Ni-Al_2O_3 under $\sigma^{\infty}=0$, $q^{\infty}=1$, $\rho=\pi/2$, where (a) $h=0$ (b) $d=0$ (c) $r=1.1$

crack as seen in Figs. 19 and 20 except the Fig. 19(c). In Fig. 19(c), Ω continuously varies from a maximum to minimum value with θ indicating the location of the crack at the same distance from the inclusion. The sudden change of Ω in Fig. 19(b) seems to be insignificant in a practical sense since K_{II} is very small and changes its sign.

4. Conclusion

The problem of a crack around an inclusion in an infinite matrix under the remote mechanical loading and heat flux is solved. The proposed method is based on the complex potential theory and dislocation functions which are used to formulate the crack problem. The resulting singular integral equations are transformed into the set of linear algebraic equations so that the unknown dislocation functions and the SIFs at the crack tip can be numerically calculated.

To investigate the interactions between the inclusion and the crack embedded in the matrix, the SIFs for various conditions (various values of γ_G, γ_A, γ_k, σ^{∞}, q^{∞}, ω, ρ, the location of the crack) are computed. Then, we analyze the crack behaviors in the engineering composite materials (SiC-Al and Ni-Al_2O_3) by obtaining the SIFs at the crack tip in composites and investigating mode mixity, i.e., the ratio of K_I and K_{II}, which is a major factor in the determination of the kink angle for the crack growth.

We summarized the results for the types of the remote loadings as follows:

(i) Under the remote mechanical tension

It is found that K_I for the case of $\gamma_G>1$ decreases as the crack gets closer to the inclusion. The magnitude of K_I is dominant for $\omega=\pi/2$ at the most locations of the crack while K_I and K_{II} are of almost same magnitude for $\omega=\pi/4$. It is found that there are some locations where the energy release rate $\mathscr{G}$ $(\sim K_I^2+K_{II}^2)$ is effectively zero. The kink angle Ω obtained from the calculated SIFs under the remote mechanical tension with $\omega=\pi/2$ shows that the crack in SiC-Al kinks away from the inclusion while it kinks toward the inclusion in Ni-Al_2O_3.

(ii) Under the remote heat flux

The effect of γ_A on SIFs is significant only near the inclusion while that of γ_k is long-ranged compared to other material property ratios γ_A and γ_G.

Acknowledgment

This research was supported by KOSEF (The Korea Science and Engineering Foundation) through CEPM (Center for Electronic Packaging Materials) at KAIST.

References

Atkinson, C., 1972, "The Interaction Between a Crack and an Inclusion," *International Journal of Engineering Science*, Vol. 10, pp. 127~136.

Bogdanoff, J. L., 1954, "Note on Thernal Stress," *Journal of Applied Mechanics*, Vol. 21, p. 88.

Cha, Y. H., Kim, K. S. and Kim, D. J., 1998, "Evaluation on the Fracture Toughness and Strength of Fiber Reinforced Brittle Matrix Composites," *KSME International Journal*, Vol. 12, No. 3, pp. 370~379.

Chao, C. K. and Lee, J. Y., 1996, "Interaction Between a Crack and a Circular Elastic Inclusion Under Remote Uniform Heat Flow," *International Journal of Solids Structures*, Vol. 33, No. 26, pp. 3865~3880.

Chung, D. Y., Huh, M. S. and Earmme, Y. Y., 2001, "Thermoelastic Interaction Between a Crack and a Circular Inhomogeneity," *International Journal of Fracture*, Vol. 111, pp. L9~L14.

Dvorak, G. J., 2000, "Composite Materials: Inelastic Behavior, Damage, Fatigue and Fracture," *International Journal of Solids and Structares*, Vol. 37, pp. 155~170.

Florence, A. L. and Goodier, J. N., 1960, "Thermal stresses due to Disturbance of Uniform Heat Flow by an Insulated Ovaloid Hole," ASME Journal of Applied Mechanics, Vol. 27, pp. 635~639.

Han, N. L., Wang, Z. G., Zhang, G. D. and Lui, L., 1999, "Effect of Reinforcement on Cyclic Stress Response of a Particulate SiC/Al Composite," *Materials Letters*, Vol. 38, pp. 70~76.

Hills, D. A., Kelly, P. A., Dai, D. N. and Korsunsky, A. M., 1996, *Solutions of Crack Problems, the Distributed Dislocation Technique*, Kluwer Academic Publishers, pp. 29~68.

Hutchinson, J. W. and Suo, Z., 1990, Mixed Mode Crocking in Layered Materials, MECH-164, Harvard University.

Jin, Z-H. and Batra, R. C., 1999, "Thermal Shock Cracking in a Metal-Particle-Reinforced Ceramic Matrix Composite," *Engineering Fracture Mechanics*, Vol. 62, pp. 339~350.

Lee, K. W., Choi, S. T. and Earmme, Y. Y., 1999, "A Circular Inhomogeneity Problem Revisited," *ASME Journal of Applied Mechanics*, Vol. 66, pp. 276~278.

Monagan, M. B., Geddes, K. O., Heal, K. M., Labahn, G., Vorkoetter, S. M., McCarron, J. and DeMarco, P., 2001, *Maple 7 Programming guide*, Waterloo Maple Inc.

Muskhelishvili, N. I., 1953, Some Basic Problems of Mathematical Theory of Elasticity, Noordhoff, Groningen.

Perlman, A. B. and Sih, G. G., 1967, "Elastostatic Problems of Curvilinear Cracks in Bonded Dissimilar Materials," *International Journal of Engineering Science*, Vol. 5, pp. 845~867.

Appendix A

The solution for the problem of an inclusion located in an infinite matrix without a crack under the remote mechanical tension is presented here as below.

We start with the equations of Perlman and Sih (1967) with the present notation

$$\Phi_M^A(z)=\begin{cases}\dfrac{1+\beta}{2}\left[F(z)+\dfrac{1+\alpha}{1-\alpha}G(z)\right], & z\in S_1\\ \dfrac{1+\beta}{2}\left[\dfrac{1-\beta}{1+\beta}F(z)+G(z)\right], & z\in S_2\end{cases}\tag{A1}$$

$$\Omega_M^A(z)=\begin{cases}\dfrac{1+\beta}{2}\left[\dfrac{1-\beta}{1+\beta}F(z)-\dfrac{1+\alpha}{1-\alpha}G(z)\right], & z\in S_1\\ \dfrac{1+\beta}{2}[F(z)-G(z)], & z\in S_2\end{cases}\tag{A2}$$

where, $F(z)=d_0+\frac{d_2}{z^2}$, $G(z)=e_0+\frac{e_2}{z^2}$, α, β are Dundurs parameters, and the subscript M denotes the mechanical loading case.

To obtain the unknowns, d_0, d_2, e_0, and e_2, we use the holomorphic conditions for $\Phi_M^A(z)$, $z\in S_1$ and $\Psi_M^A(z)$ $z\in S_1$ and the asymptotic behavior of $\Phi_M^A(z)$, $z\in S_2$ and $\Psi_M^A(z)$, $z\in S_2$. Since the work by Perlman and Sih (1967) contains some errors in obtaining the unknowns, we derived the correct solution as follows:

Equation (A1) is rewritten as

$$\Phi_M^A(z)=\frac{1+\beta}{2}\left[d_0+\frac{d_2}{z^2}+\frac{1+\alpha}{1-\alpha}\times\left(e_0+\frac{e_2}{z^2}\right)\right] \quad \text{(A1-1)}$$

whence the requirement of the non-singularity at $z=0$ yields

$$d_2+\frac{1+\alpha}{1-\alpha}e_2=0 \quad \text{(A3)}$$

We have the relation

$$\Psi_M^A(z)=\frac{1}{z^2}\left[\Phi_M^A(z)-z\Phi_M'^A(z)-\bar{\Omega}_M^A\left(\frac{1}{z}\right)\right] \quad \text{(A4)}$$

hence we can obtain in an analogous way to the derivation of Eq. (A3)

$$\frac{\beta}{1+\beta}d_0+\frac{1+\alpha}{1-\alpha}e_0=0 \quad \text{(A5)}$$

which originates from the holomorphic condition of $\Psi(z)$ at $z=0$.

On the other hand, the asymptotic behavior of $\Phi_M^A(z)$, $z\in S_2$ and $\Psi_M^A(z)$, $z\in S_2$ is written as

$$\Phi_M^A(z)=\frac{\sigma^\infty}{4}+\frac{a_1}{z}+\frac{a_2}{z^2}+\cdots, \qquad z\in S_2 \quad \text{(A6)}$$

$$\Psi_M^A(z)=\frac{-\sigma^\infty}{2}e^{-2i\omega}+\frac{b_1}{z}+\frac{b_2}{z^2}+\cdots, \quad z\in S_2 \quad \text{(A7)}$$

Equation (A6) and (A7) are substituted into Eq. (A4), to obtain the asymptotic behavior of $\Omega_M^A(z)$. By comparing the coefficients of constants in Eq. (A1) and (A2), respectively with (A6) and the expression $\Omega_M^A(z)$, described above we get

$$\frac{\sigma^\infty}{4}=\frac{(1-\beta)}{2}d_0+\frac{(1+\beta)}{2}e_0 \quad \text{(A8)}$$

$$d_2-e_2=\frac{-\sigma^\infty}{(1+\beta)}e^{2i\omega} \quad \text{(A9)}$$

From Eq. (A3) and Eq. (A9), we have

$$e_2=\frac{\sigma^\infty}{2}\frac{(1-\alpha)}{(1+\beta)}e^{2i\omega} \quad \text{(A10)}$$

$$d_2=\frac{-\sigma^\infty}{2}\frac{(1+\alpha)}{(1+\beta)}e^{2i\omega} \quad \text{(A11)}$$

Also from Eq. (A5) and Eq. (A8), we have

$$d_0=\frac{\sigma^\infty}{2}\frac{(1+\alpha)}{(1+\alpha-2\beta)} \quad \text{(A12)}$$

$$e_0=\frac{-\sigma^\infty}{2}\frac{(1-\alpha)}{(1+\alpha-2\beta)}\frac{\beta}{(1+\beta)} \quad \text{(A13)}$$

By substituting Eqs. (A10) ~ (A13) into Eqs. (A1) ~ (A2), the followings are obtained:

$$\Phi_M^A(z)=\begin{cases}\dfrac{(1+\alpha)}{(1+\alpha-2\beta)}\dfrac{\sigma^\infty}{4}, & z\in S_1\\ \dfrac{\sigma^\infty}{4}+\dfrac{(\alpha-\beta)}{(1+\beta)}\dfrac{\sigma^\infty}{2}\dfrac{e^{2i\omega}}{z^2}, & z\in S_2\end{cases} \quad \text{(A14)}$$

$$\Omega_M^A(z)=\begin{cases}\dfrac{(1+\alpha)}{(1+\alpha-2\beta)}\dfrac{\sigma^\infty}{4}+\dfrac{(1+\alpha)}{(1+\beta)}\dfrac{\sigma^\infty}{2}e^{2i\omega}\dfrac{1}{z^2}, & z\in S_1\\ \dfrac{1+\alpha+2\beta}{1+\alpha-2\beta}\dfrac{\sigma^\infty}{4}+\dfrac{\sigma^\infty}{2}\dfrac{e^{2i\omega}}{z^2}, & z\in S_2\end{cases} \quad \text{(A15)}$$

Eqs. (A14) ~ (A15) represent the terms due to the mechanical loading on the right hand side of Eqs. (5) ~ (6), respectively.